International Journal of Networking and Computing – www.ijnc.org, ISSN 2185-2847
Volume 9, Number 2, pages 354–369, July 2019

Relation between spatio-temporal patterns generated by two-dimensional cellular automata and a singular function

Akane KAWAHARADA
Department of Mathematics, Kyoto University of Education
1 Fujinomori-cho, Fukakusa, Fushimi-ku, Kyoto, 612-8522, JAPAN

Takao NAMIKI
Department of Mathematics, Hokkaido University
Kita 10, Nishi 8, Kita-ku, Sapporo, Hokkaido, 060-0810, JAPAN

Received: October 26, 2018
Revised: April 7, 2019
Revised: May 7, 2019
Accepted: May 7, 2019
Communicated by Yasuyuki Nogami

Abstract

In this study, we examine the relation between the spatio-temporal patterns generated by two-dimensional symmetrical elementary cellular automata and a singular function. In a previous paper, we proved that a specific cellular automaton admits a "limit set" (a limit on the series of spatio-temporal patterns contracted with time), and we calculated the fractal dimension of the boundary of this limit set. In this paper, we provide an overview of the previous results and a more precise analysis. Numerical simulations demonstrate that the essential fractal-like patterns created by two-dimensional cellular automata are also related to a singular function.

Keywords: two-dimensional symmetrical elementary cellular automata, fractal geometry, singular function

1 Introduction

The relation between cellular automata and fractal geometry has been studied mathematically for many years. In the 1980s, Willson proved that for linear cases one-dimensional linear cellular automata with a prime number of states admit a limit set under a suitable scaling [1]. Takahashi studied the dimension spectra of linear cellular automata [2]. However, it is difficult to apply this analysis to nonlinear cellular automata, and not even a case study has been presented on this topic for some time. Kawaharada studied a two-dimensional nonlinear cellular automaton that generates a spatio-temporal pattern with a fractal structure [3]. It was found that a family of unstable invariant sets exists for which the dynamics are conjugate to the one-dimensional elementary cellular automaton Rule 150 [3]. A further study demonstrated that the automaton admits a limit set starting from a certain initial configuration, and showed the box-counting dimension of its boundary [4]. This demonstrated the relation between a two-dimensional cellular automaton and a singular function.

It is well known that there exist many types of fractal curves that have pathological features [5]. For example, the Weierstrass function and the Takagi function (also known as the Blancmange

curve) are continuous everywhere but not differentiable anywhere. However, singular functions are continuous everywhere and differentiable almost everywhere [5–7]. The number of "0" states in the configuration of a two-dimensional nonlinear cellular automaton has been studied numerically, as shown in Figure 1 [3,8]. We can observe that the number of "0" states at each time step is described well by a singular function, which comprises a self-affine function on a unit interval. We show that the spatio-temporal pattern of the cellular automaton is related to this singular function, instead of directly calculating its fractal dimension. This result indicates that the pattern itself is also fractal.

Based on these previous studies, we consider a characterization of the fractal structures of spatial or spatio-temporal patterns regardless of the linearity of a cellular automaton. In this study, we replace the spatial or spatio-temporal patterns of a nonlinear cellular automaton by the unions of squares. We show that the dynamics of the area of the union are represented by a singular function, and we obtain the fractal dimension (herein, we consider the box-counting dimension) of a spatial pattern by calculating the area of the union of squares. Further, we focus on cellular automata that are two-dimensional, symmetrical, and elementary. Numerical simulations show that there exist 1024 automata that create important patterns with fractal structures. It is also shown that some of the patterns are related to the singular functions. For six of the patterns, the number of "0" states at each time step is described by a singular function, which represents a generalization of a result for a particular cellular automaton [3,8]. In addition, for two of the patterns the cumulative sum of the number of "0" states is also described by this function. These results indicate that the singular function is strongly associated with cellular automata.

The remainder of the paper is organized as follows. Section 2 describes the prerequisites concerning cellular automata and singular functions. In Section 3, we provide an overview of previously derived results [4], and present a more precise calculation. In Section 4, numerical results are presented. We study the spatio-temporal patterns generated by symmetrical two-dimensional cellular automata, and establish their relation to the singular function. The results reveal that the cellular automata have a deep relation not only with fractal geometry, but also with singular functions. Finally, Section 5 presents a discussion and describes possible areas for future studies.

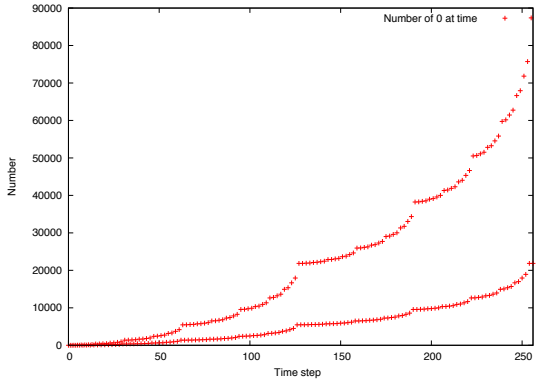

Figure 1: The number of "0" states in a configuration of the cellular automaton for the time steps $0 \leq n \leq 256$. The behavior is different for the odd and even n cases. The upper curve of the graph represents the odd n cases and the lower one represents the even n cases.

2 Prerequisites

In this section, we present some definitions and notations for symmetrical two-dimensional elementary cellular automata and singular functions.

2.1 Symmetrical two-dimensional elementary cellular automata

Suppose that (X, F) is a discrete dynamical system consisting of a space X and a transformation F on X. The n-th iterate of F is denoted by F^n. Thus, F^0 is the identity map on X. Let $A = \{0, 1\}$ be a binary state set and $A^{\mathbb{Z}^2}$ be the two-dimensional configuration space. We call the configuration $x_o \in A^{\mathbb{Z}^2}$ such that

$$(x_o)_{i,j} = \begin{cases} 0 & \text{if } (i,j) = (0,0), \\ 1 & \text{if } (i,j) \in \mathbb{Z}^2 \backslash \{(0,0)\}, \end{cases} \tag{1}$$

a **single site seed**. In this article, we consider the orbits from a single site seed as an initial configuration.

We next define two-dimensional elementary cellular automata.

Definition 2.1. *1.* **A two-dimensional elementary cellular automaton (2dECA)** $(A^{\mathbb{Z}^2}, F)$ *is given by*

$$(Fx)_{i,j} = f\begin{pmatrix} & x_{i,j+1} & \\ x_{i-1,j} & x_{i,j} & x_{i+1,j} \\ & x_{i,j-1} & \end{pmatrix} = f\begin{pmatrix} T \\ LCR \\ B \end{pmatrix} \tag{2}$$

for any coordinate $(i, j) \in \mathbb{Z}^2$ and $x \in A^{\mathbb{Z}^2}$, where $f : A^5 \to A$ is a map depending on the five states of the von Neumann neighborhood. We name f a **local rule**.

2. A 2dECA $(A^{\mathbb{Z}^2}, F)$ is a **symmetrical 2dECA (Sym-2dECA)** *if the local rule f satisfies the following conditions:*

$$f\begin{pmatrix} T \\ LCR \\ B \end{pmatrix} = f\begin{pmatrix} B \\ LCR \\ T \end{pmatrix} = f\begin{pmatrix} T \\ RCL \\ B \end{pmatrix}, \ f\begin{pmatrix} T \\ LCR \\ B \end{pmatrix} = f\begin{pmatrix} L \\ BCT \\ R \end{pmatrix} = f\begin{pmatrix} B \\ RCL \\ T \end{pmatrix} = f\begin{pmatrix} R \\ TCB \\ L \end{pmatrix}. \tag{3}$$

The first equality of (3) provides the left-right and top-bottom symmetry and the second gives the rotational symmetry of the local rule. We can easily prove that 2^{32} 2dECAs exist, among which $2^{12}(= 4096)$ are Sym-2dECAs. The local rule of a Sym-2dECA can be obtained from a combination of only 12 transitions for

$$\begin{pmatrix} 0 \\ 000 \\ 0 \end{pmatrix}, \begin{pmatrix} 0 \\ 000 \\ 1 \end{pmatrix}, \begin{pmatrix} 0 \\ 001 \\ 1 \end{pmatrix}, \begin{pmatrix} 1 \\ 000 \\ 1 \end{pmatrix}, \begin{pmatrix} 0 \\ 101 \\ 1 \end{pmatrix}, \begin{pmatrix} 1 \\ 101 \\ 1 \end{pmatrix}, \begin{pmatrix} 0 \\ 010 \\ 0 \end{pmatrix}, \begin{pmatrix} 0 \\ 010 \\ 1 \end{pmatrix}, \begin{pmatrix} 0 \\ 011 \\ 1 \end{pmatrix}, \begin{pmatrix} 1 \\ 010 \\ 1 \end{pmatrix}, \begin{pmatrix} 0 \\ 111 \\ 1 \end{pmatrix}, \begin{pmatrix} 1 \\ 111 \\ 1 \end{pmatrix}. \tag{4}$$

2.2 A Sym-2dECA as a modified Ulam's cell model

Here, we introduce a particular Sym-2dECA $(A^{\mathbb{Z}^2}, T)$.

Definition 2.2. *The rule of the Sym-2dECA $(A^{\mathbb{Z}^2}, T)$ is defined by*

$$(Tx)_{i,j} = x_{i,j} + x_{i-1,j}x_{i+1,j} + x_{i,j-1}x_{i,j+1} \pmod 2 \tag{5}$$

for each coordinate $(i, j) \in \mathbb{Z}^2$ and any $x \in A^{\mathbb{Z}^2}$.

This CA is a nonlinear CA, because the second and third terms of the local rule are the products of two states. This local rule is also given in Table 1.

Table 1: Local rule of the CA given by (5) as a Sym-2dECA. This rule is a particular case of $\langle 10c \rangle$ in Table 2

T	0	0	0	1	0	1	0	0	0	1	0	1
LCR	000	000	001	000	101	101	010	010	011	010	111	111
B	0	1	1	1	1	1	0	1	1	1	1	1
$(Tx)_{i,j}$	0	0	0	1	1	0	1	1	1	0	0	1

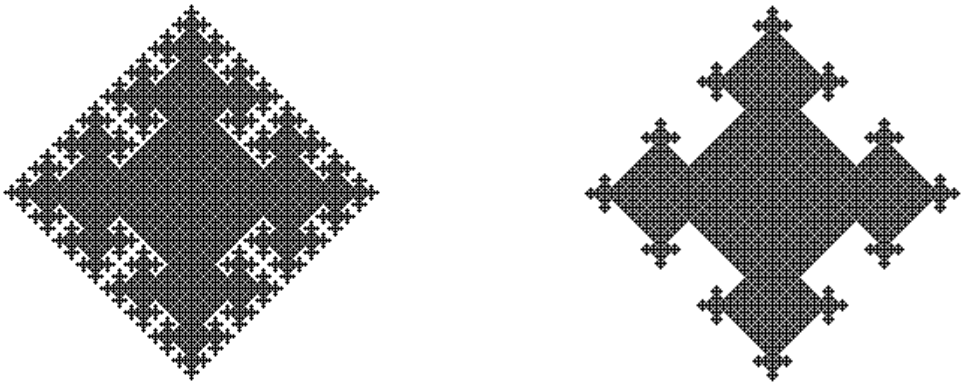

(a) $T^{125}x_o$ (b) $T^{107}x_o$

Figure 2: Configurations $T^{125}x_o$ and $T^{107}x_o$ of the CA $(A^{\mathbb{Z}^2}, T)$. A black dot represents the state "0," and a white dot "1." A fine structure can be observed on the boundary.

Figure 2 presents patterns of a nonlinear two-dimensional CA for the time steps 125 and 107. The spatial patterns of the CA started from a single site seed x_o, as defined in Equation 1. A black dot represents the state "0," and a white dot "1." The patterns shown in Figure 10 $\langle 10c \rangle$ have also evolved from the time steps 8 to 15. In these pictures, a black dot represents the state "0" and a white dot represents the state "1."

The CA is related to Ulam's cell-model, which is employed to study the formation of crystalline patterns [9]. Ulam studied the model to construct a simpler model that creates fractal-like crystalline patterns. In this model, the existing cells never die during the time evolution. For a particular initial configuration x_o, $\{T^{2n-1}x_o\}_{n=1}^{\infty}$ is exactly the same as the spatio-temporal pattern of Ulam's cell model, so that the "0" states never turn to the "1" states. The spatio-temporal patterns of an even number of iterations $\{T^{2n}x_o\}_{n=0}^{\infty}$ are different from those of an odd number of iterations $\{T^{2n-1}x_o\}_{n=1}^{\infty}$. The relation between the two spatio-temporal patterns has been demonstrated numerically [3]. The number of "0" state cells in $T^{2n-1}x_o$ is the same as in $T^{4n-2}x_o$. Thus, we consider only the former case. Kawaharada demonstrated the relation between the one-dimensional elementary cellular automaton Rule150 and the CA $(A^{\mathbb{Z}^2}, T)$ [3]. The subdynamics of the CA are equivalent to Rule 150.

2.3 Singular function

Here, we introduce a self-affine function on the unit interval. This function is an example of a fractal curve. Let α be a parameter such that $0 < \alpha < 1$ and $\alpha \neq 1/2$.

Definition 2.3 ([5, 10]). **The singular function** $L_\alpha : [0,1] \to [0,1]$ *is defined as follows:*

$$L_\alpha(x) := \begin{cases} \alpha L_\alpha(2x) & (0 \leq x < 1/2), \\ (1-\alpha)L_\alpha(2x-1) + \alpha & (1/2 \leq x \leq 1). \end{cases} \tag{6}$$

The functional equation has a unique continuous solution on $[0,1]$. The graph of L_α with $\alpha = 1/4$ is presented in Figure 3. It is known that the function is strictly increasing on $[0,1]$ and that its derivative is zero almost everywhere. Kawamura [11] derived the set in which the derivative of the function is zero. In this paper, "singular function" refers to the function defined by the functional equation (6). This function L_α has been studied by many researchers [7, 10, 12].

Now, we introduce an additional definition [5]. We consider flipping a coin with the probability $\alpha \in (0,1)$ for heads and a probability $1-\alpha$ for tails, where we assume that $\alpha \neq 1/2$. The binary expansion of $x \in [0,1]$ is determined by flipping the coin infinitely, $x = \sum_{n=1}^{\infty} x_n/2^n$, where each

x_n is 0 or 1 as determined by the n-th toss. Then, the singular function $L_\alpha : [0,1] \to [0,1]$ is also defined by the distribution function of x:

$$L_\alpha(t) := prob\{x \le t\} \quad (0 \le t \le 1). \tag{7}$$

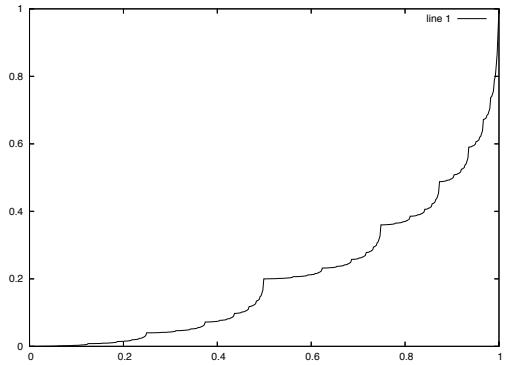

Figure 3: Graph of the singular function L_α with the parameter $\alpha = 1/4$ defined by eq. (6).

3 Analysis of the fractal structures of a particular Sym-2dECA

In this section, we study the fractal structure of the Sym-2dECA $(A^{\mathbb{Z}^2}, T)$ (5). We present the prefractal sets $\{K_n\}$, and characterize the sets by the singular function. We also show the existence of the "limit set" and calculate the box-counting dimension of the boundary of this limit set.

3.1 Prefractal sets $\{K_n\}$ representing the fractal structure of the Sym-2dECA

We construct the prefractal sets $\{K_n\}$ on the two-dimensional Euclidean space $\mathbb{R}^2$.

To simplify, we will identify each "0" state of a configuration as a square, in the following manner. In a configuration $x \in A^{\mathbb{Z}^2}$, if $x_{i,j} = 0$ for a certain coordinate $(i,j) \in \mathbb{Z}^2$ then we replace the state "0" with a 45 degree rotated square with the vertices $(i-1,j)$, $(i+1,j)$, $(i,j+1)$, and $(i,j-1)$. Then, we have a combination of squares instead of lattice points (see Figure 4). In the configuration x, if $x_{i,j} = 0$, $x_{i\pm1,j} = 1$, and $x_{i,j\pm1} = 1$, then the center state "0" is converted to one square with a side length of $\sqrt{2}$.

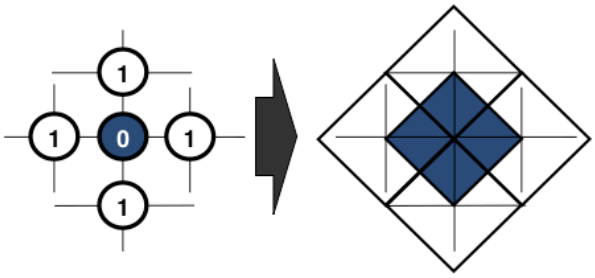

Figure 4: Result when $x_{i,j} = 0$, $x_{i\pm1,j} = 1$, and $x_{i,j\pm1} = 1$.

Next, we define an increasing sequence $\{K_n\}$, which comprises the union of these squares.

Definition 3.1. *A family of prefractal sets $\{K_n\}$ is given for each natural number n.*

1. *For $n = 2^k$ ($k = 0, 1, 2, 3, \dots$), the set K_{2^k} is a square centered at the origin with the coordinates of its vertices being $(2^{k+1}, 0)$, $(-2^{k+1}, 0)$, $(0, 2^{k+1})$, and $(0, -2^{k+1})$.*

2. *For n with $2^k < n < 2^{k+1}$, we define K_n in the following manner. Using the binary expansion of n, we have*

$$n = 2^{l_N} + 2^{l_{N-1}} + \cdots + 2^{l_1} + 2^{l_0}, \tag{8}$$

where $\{l_j\}_{j=0}^{N}$ is an increasing sequence and $l_N = k$. We place a $K_{2^{l_{N-1}}}$ centered at each of the four vertices of K_{2^k}. We call the resulting figure $K_{2^k+2^{l_{N-1}}}$. Next, we place a $K_{2^{l_{N-2}}}$ centered at each of the 12 vertices of $K_{2^k+2^{l_{N-1}}}$, and we call the resulting figure $K_{2^k+2^{l_{N-1}}+2^{l_{N-2}}}$. For $K_{2^k+2^{l_{N-1}}+\cdots+2^{l_{N-J}}}$ ($J \in \{0, 1, \dots, N\}$), the number of vertices is $4 \cdot 3^J$. Inductively, we can define K_n for every n uniquely.

From previous observations [3,8], we notice that for the Sym-2dECA K_n represents the structure of $T^{2n-1}x_o$. If $n = 2^k$ for each natural number k, then the pattern of $T^{2n-1}x_o$ is simply in a basic square. If $2^k < n < 2^{k+1}$, then the pattern is the union of T^{2^k} and some parts of $T^{(2n-1)-2^k}$. Figure 5 shows the configurations $T^{2n-1}x_o$ and prefractal sets K_n for $n = 32$, 48, 52, and 54. We can observe that K_n is a good representation of $T^{2n-1}x_o$.

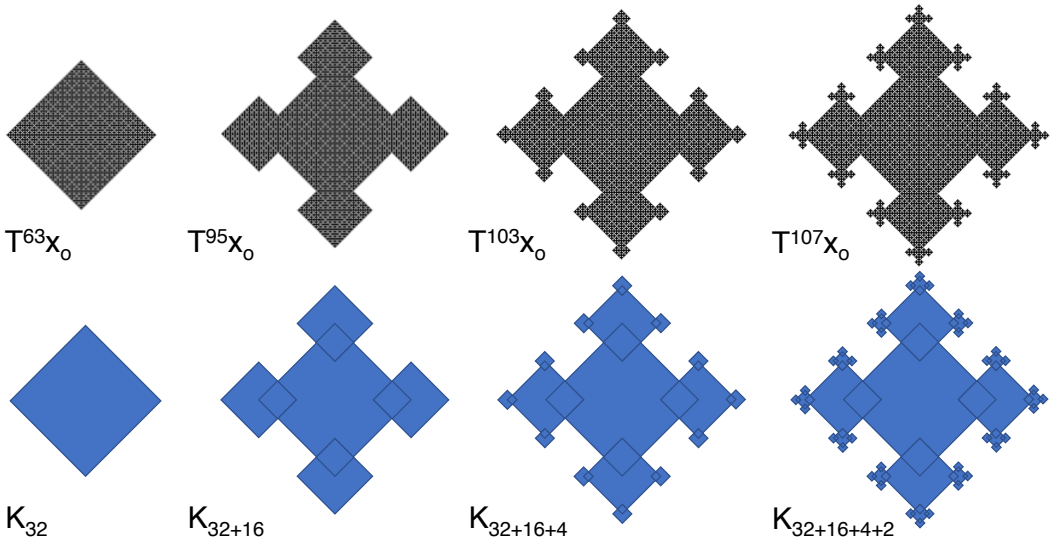

Figure 5: Figure for $K_{54} = K_{2^5+2^4+2^2+2^1}$.

Example 3.1. *We construct K_{54} for the structure $T^{107}x_o$ (b) in Figure 2 using the following procedure (see Figure 5). From the binary expansion of 54, we have that $54 = 2^5 + 2^4 + 2^2 + 2^1$. We place K_{2^5} on a square centered at the origin, with the coordinates of its vertices as $(2^6, 0)$, $(-2^6, 0)$, $(0, 2^6)$, and $(0, -2^6)$. Next, we place K_{2^4} centered at each of the four vertices of K_{2^5}. Then, we obtain the figure $K_{2^5+2^4}$. Inductively, we place K_{2^2} centered at each of the $12 (= 4 \cdot 3)$ vertices of $K_{2^5+2^4}$, and place K_{2^1} centered at each of the $36 (= 4 \cdot 3^2)$ vertices of $K_{2^5+2^4+2^2}$. Finally, we obtain $K_{2^5+2^4+2^2+2^1}$.*

3.2 Area of K_n and the singular function L_α

As in Example 3.1, for the Sym-2dECA $(A^{\mathbb{Z}^2}, T)$ the prefractal set K_n represents the structure of a configuration $T^{2n-1}x_o$. Hereafter, we will estimate the area of K_n, and illustrate the relation between the CA and the singular function.

For a natural number n, $n = \sum_{j=0}^{N} 2^{l_j}$ with an increasing sequence $\{l_j\}_{j=0}^{N}$ by the binary expansion. Define $m = l_N$ (we have $n < 2^{m+1}$). From the definition of $\{K_n\}$, $K_{n+2^{m+1}}$ is constructed by

placing $K_{2^{m+1}}$ first, and then four K_n sets centered on each vertex of $K_{2^{m+1}}$. Define $S(n)$ as the area of K_n. Then we have that

$$S(n+2^{m+1}) = S(2^{m+1}) + 4 \times \frac{3}{4} S(n) = S(2^{m+1}) + 3S(n). \tag{9}$$

Example 3.2. *We calculate $S(54)$. Figure 6 shows the areas $S(6)$, $S(22)$, and $S(54)$. By Definition 3.1, $K(2^k)$ for $k \in \mathbb{N}$ is a simple square. First, we have that $S(6) = S(2^2) + 4 \times \frac{3}{4}S(2)$, because we notice from Figure 6(a) that $S(6)$ is divided by a square $S(2^2)$ and four copies of $\frac{3}{4}S(2)$. Next, $S(22)$ in Figure 6(b) is represented by a square $S(2^4)$ and four copies of $\frac{3}{4}S(6)$, and we have that $S(54) = S(2^5) + 4 \times \frac{3}{4}S(22)$ by a similar argument.*

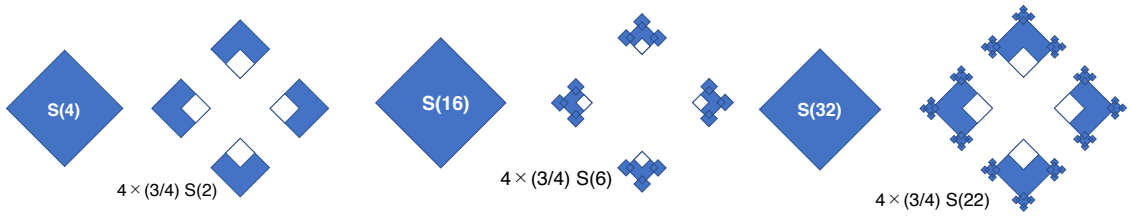

(a) $S(6)$ (b) $S(22)$ (c) $S(54)$

Figure 6: Area of $K(n)$.

Using the same procedure, it is easy to see that $S(n+2^{m+i}) = S(2^{m+i}) + 3S(n)$ for any natural number i. As a result, $S(n) = \sum_{j=0}^{N} 3^{N-j} S(2^{l_j})$, and $S(2^i) = 2(2^{i+1})^2$ for all i. Therefore, we have that $S(n) = 2\sum_{j=0}^{N} 3^{N-j} 2^{2(l_j+1)}$. Scaling by $S(2^{m+1}) = 2 \cdot 2^{2(m+2)}$ gives the following:

$$\frac{S(n)}{S(2^{m+1})} = \sum_{j=0}^{N} 3^{N-j} 2^{2(l_j-m-1)}. \tag{10}$$

Moreover, we have the following theorem:

Theorem 3.1. *Consider a rational $x \in [0,1)$ of the form $p/2^{m+1}$, and let $\{l_j\}_{j=0}^{N}$ be a strictly increasing sequence of exponents in the binary expansion of p such that $p = \sum_{j=0}^{N} 2^{l_j}$ and $x = \sum_{j=0}^{N} 2^{l_j-m-1}$. Then, $\sum_{j=0}^{N} 3^{N-j} 2^{2(l_j-m-1)} = L_{1/4}(x)$.*

It is clear that if we set $g(x) := \sum_{j=0}^{N} 3^{N-j} 2^{2(l_j-m-1)}$, then $g(2x-1) = \sum_{j=0}^{N-1} 3^{N-j-1} 2^{2(l_j-m)}$. Thus, we have that

$$\frac{3}{4} g(2x-1) + \frac{1}{4} = \Big(\sum_{j=0}^{N-1} 3^{N-j} 2^{2(l_j-m-1)} \Big) + \Big(3^{N-N} 2^{2(l_N-m-1)} \Big) = g(x). \tag{11}$$

This relationship is the functional equation of the singular function $L_{1/4}$ (6) for rational $x \in [0,1)$.

Remark 3.1. *In the previous papers [3,8], it was suggested that the number of "0" states in $T^{2n-1}x_o$ was related to the singular function $L_{1/4}$. Theorem 3.1 proves these results.*

3.3 Box-counting dimension of fractal sets generated by $\{K_n\}$

First, we define the box-counting dimension and the limit set.

Fractals are mathematical objects whose fractal dimension is not an integer. A fractal dimension is a measure of the complexity of a pattern. The box-counting dimension is useful for calculating or estimating these dimensions.

Let U be a nonempty bounded subset of $\mathbb{R}^D$, which is a D-dimensional Euclidean space, and let $N_\delta(U)$ be the smallest number of copies of a ball of radius δ necessary to cover U. Thus, $N_\delta(U) < \infty$.

Definition 3.2 ([14]). **The box-counting dimension** $\dim_B$ *of* U *is defined by*

$$\dim_B(U) := \lim_{\delta \to 0} \frac{\log N_\delta(U)}{-\log \delta}, \tag{12}$$

if the limit exists.

This definition means that for the grid size δ we count the number of intersecting cells. As the grid becomes finer, we can observe how this number changes. If the limit exists, then this is the box-counting dimension. Here, we calculate the box-counting dimension of the boundary of $T^{2n-1}x_o$ for the Sym-2dECA (5). For n, we have that $a = (\cdots a_3a_2a_1a_0) = \{a_i\}_{i\in\mathbb{N}} \in A^{\mathbb{N}}$ such that the binary expansion of n is $\sum_{i=0}^{\infty} a_i 2^i$. Let $n_m = \sum_{i=0}^{m} a_i 2^i$ ($a_m = 1$). Furthermore, for a given $a = \{a_i\}_{i\in\mathbb{N}}$, let $\{m_k\}_{k=0}^{\infty}$ be an increasing sequence determined by $a_{m_k} = 1$. Then, we have an infinite sequence $\{K_{n_{m_k}}\}$ based on Definition 3.1 where $n_{m_k} = \sum_{i=0}^{m_k} a_i 2^i$. We define the limit set of $\{K_{n_{m_k}}/2^{m_k+1}\}$, which is a subset of the two-dimensional Euclidean space $\mathbb{R}^2$, as follows, where set $K_{n_{m_k}}/2^{m_k+1}$ denotes the contracted set of $K_{n_{m_k}}$ by the rate $1/2^{m_k+1}$, and is defined by $\{(i/2^{m_k+1}, j/2^{m_k+1}) \in \mathbb{R}^2 \mid (i,j) \in K_{n_{m_k}} \subset \mathbb{R}^2\}$.

Definition 3.3 ([15]). **The limit set** *for the sequence of configurations* $\{T^{2n_{m_k}-1}x_o\}$ *for the Sym-2dECA* $(A^{\mathbb{Z}^2}, T)$ *is defined by*

$$\lim_{k\to\infty} \frac{K_{n_{m_k}}}{2^{m_k+1}}, \tag{13}$$

if it exists.

Next, we discuss the box-counting dimension of the boundary of the limit set $\{K_{n_{m_k}}/2^{m_k+1}\}$ $(k \to \infty)$.

First, we observe the step from $K_{n_{m_k}}$ to $K_{n_{m_{k+1}}}$ through the example: $4 = 100|_2 \to 12 = 1100|_2 \to 28 = 11100|_2 \to \cdots$. In this example, $m_0 = 2$, $m_1 = 3$, and $m_2 = 4$.

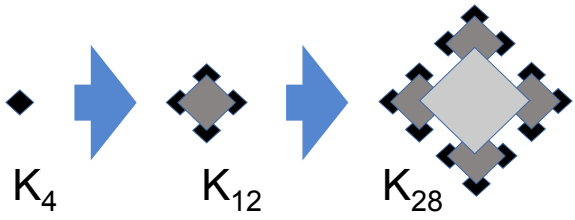

Figure 7: Figures for $K_{n_{m_k}}$: K_4 ($n_{m_0} = n_2 = 4$), K_{12} ($n_{m_1} = n_3 = 12$), and K_{28} ($n_{m_2} = n_4 = 28$), sequentially.

We denote the length of the boundary of K_n by $l(n)$. For the example in Figure 7, we have that $l(12) = 4\frac{3}{4}l(4) + (l(8) - l(4))$ and $l(28) = 3l(12) + (l(16) - l(8))$. In general,

$$l(n_{m_{k+1}}) = 3l(n_{m_k}) + \big(l(2^{m_{k+1}}) - l(2^{m_k})\big). \tag{14}$$

Finally,

$$\begin{aligned}
l(n_{m_{k+1}}) &= 3^k l(n_{m_1}) + \big(l(2^{m_{k+1}}) - l(2^{m_k})\big) + 3\big(l(2^{m_k}) - l(2^{m_{k-1}})\big) + \cdots + 3^k\big(l(2^{m_1}) - l(2^{m_0})\big) \\
&= 3^k l(n_{m_1}) + \sum_{i=0}^{k} \Big(3^i l(2^{m_{k+1-i}}) - 3^i l(2^{m_{k-i}})\Big) \\
&= 3^k \Big\{ l(n_{m_1}) + \sum_{i=0}^{k} \Big(3^{i-k} l(2^{m_{k+1-i}}) - 3^{i-k} l(2^{m_{k-i}})\Big)\Big\} \\
&= 3^k \Big\{ l(n_{m_1}) + 2\sqrt{2} \sum_{i=0}^{k} \Big(3^{i-k} 2^{m_{k+1-i}} - 3^{i-k} 2^{m_{k-i}}\Big)\Big\}.
\end{aligned}$$

The right-hand side is transformed as follows:

$$
\begin{aligned}
&3^k\Big\{l(n_{m_1})+2\sqrt{2}\sum_{i=0}^{k}\Big(\exp\left((i-k)\log 3+m_{k+1-i}\log 2\right)-\exp\left((i-k)\log 3+m_{k-i}\log 2\right)\Big)\Big\}\\
&=3^k\Big\{l(n_{m_1})+2\sqrt{2}\sum_{i=0}^{k}\Big(\exp\left(-i\log 3+m_{i+1}\log 2\right)-\exp\left(-i\log 3+m_i\log 2\right)\Big)\Big\}\\
&=3^k\Big\{l(n_{m_1})+2\sqrt{2}\sum_{i=0}^{k}\Big(\exp\Big(-i(\log 3+\frac{m_{i+1}}{i}\log 2)\Big)-\exp\Big(-i(\log 3+\frac{m_i}{i}\log 2)\Big)\Big)\Big\}.
\end{aligned}
$$

We have that $l(n_{m_{k+1}})=3^k(P+Q)$, where $P=l(n_{m_1})$ and $Q=2\sqrt{2}\sum_{i=0}^{k}\Big(\exp\big(-i(\log 3+\frac{m_{i+1}}{i}\log 2)\big)-\exp\big(-i(\log 3+\frac{m_i}{i}\log 2)\big)\Big)$. Recall that our problem is to estimate the box-counting dimension of the boundary of $K:=\lim_{k\to\infty}K_{n_{m_k}}/2^{m_k+1}$, $dim_B\partial K$, under the scaling

$$
\lim_{k,m_k\to\infty}\frac{\partial K_{n_{m_k}}}{2^{m_k}}\quad\text{and}\quad\lim_{k,m_k\to\infty}\frac{l(n_{m_k})}{2^{m_k}}. \tag{15}
$$

For this, only need to estimate is the term $3^k(P+Q)/2^{m_k}$. Here, P is a constant, and Q converges if $\lim k/m_k>\log 2/\log 3$, by the ratio test. Therefore, we have that

$$
l(n_{m_{k+1}})\sim\begin{cases}3^k & \text{if } P+Q<\infty,\\ 2^{m_k} & \text{elsewhere.}\end{cases} \tag{16}
$$

From this discussion, we can see that the box-counting dimension exists if $p=\lim_{k\to\infty}k/m_k$, where m_k is the highest order of n_{m_k} and k is the number of "1" states in $a_0,a_1,\ldots,a_{m_k}$. Furthermore, the dimension is either $p\log 3/\log 2$ or 1.

In summarizing these discussions, we are led to Theorem 3.2.

Theorem 3.2. *The limit set $K=\lim_{k\to\infty}K_{n_{m_k}}/2^{m_k+1}$ exists and the box-counting dimension of the boundary of K_n, $\lim_k\partial K_{n_{m_k}}/2^{m_k+1}$, satisfies*

$$
dim_B\partial K=\begin{cases}p\dfrac{\log 3}{\log 2} & \Big(p>\dfrac{\log 2}{\log 3}\Big),\\ 1 & \Big(p\le\dfrac{\log 2}{\log 3}\Big),\end{cases} \tag{17}
$$

if $p:=\lim_{k\to\infty}k/m_k$ $(0\le p\le 1)$ exists.

Remark 3.2. *The existence of a limit set as a subset of $\mathbb{R}^2$ is clear from the inclusion property $K_{2^k}/2^{k+1}\subset K_{2^{k-1}}/2^k$.*

4 Numerical observations of fractal structures generated by Sym-2dECAs

In this section, we study the patterns of all 4096 Sym-2dECAs from a particular initial configuration: the single site seed x_o. We obtain various types of patterns. First, we classify these patterns. The local rules of Sym-2dECAs are obtained from a combination of 12 transitions. We focus on the two transitions

$$
a:=f\begin{pmatrix}0\\111\\1\end{pmatrix}\quad\text{and}\quad b:=f\begin{pmatrix}1\\111\\1\end{pmatrix}. \tag{18}
$$

When $(a,b)=(0,1)$, the conditions imply that any spatial patterns from x_o grow infinitely, and any cells outside of the spatial pattern comprising the "0" states on $F^n x_o$ are fixed by "1": $(Fx_o)^n_{i,j}=1$ if $|i|+|j|>n$ for any $n\in\mathbb{N}$. For the other cases, if $(a,b)=(0,0),(1,0),(1,1)$ then the spatial pattern $F^n x_o$ eventually falls under the following cases:

(i) Fixed or oscillating pattern with a maximum of two periods, i.e., there exists $k\in\mathbb{N}$ such that $F^{2n+k}x_o=F^{2m+k}x_o$ for any $n,m\in\mathbb{N}$;

(ii) Flipped pattern of Sym-2dECAs with $(a,b)=(0,1)$, $(A^{\mathbb{Z}^2},\tilde{F})$, i.e., for some k, $(F^{n+k}x_o)_{i,j}=1-(\tilde{F}^{n+k}x_o)_{i,j}$ for any coordinate $(i,j)\in\mathbb{Z}^2$;

(iii) Superposition of four or five spatial patterns of a Sym-2dECA with $(a,b)=(0,1)$, i.e., for some k and $(i,j)\in\mathbb{Z}^2$, $(F^{n+k}x_o)_{i,j}=\sum_{(p,q)\in V}(\tilde{F}^{n+k}(\sigma_{p,q}x_o))_{i,j}$, where $V=\{(\pm1,0),(0,\pm1)\}$ or $\{(0,0),(\pm1,0),(0,\pm1)\}$, and $\sigma_{p,q}$ with $(p,q)\in\mathbb{Z}^2$ is the shift transformation on $\mathbb{Z}^2$; and

(iv) Oscillating outside the spatial pattern with two periods, i.e., for some k, $(F^{2n+k}x_o)_{i,j}=1$ and $(F^{2n+1+k}x_o)_{i,j}=0$, where $|i|,|j|>2n+1+k$.

The patterns obtained from (i) are too simple, the patterns obtained from (ii) and (iii) are based on the patterns with $(a,b)=(0,1)$, and the patterns obtained from (iv) are too complicated to analyze. Therefore, the patterns with $(a,b)=(0,1)$ are essential to understanding the fractal structures of two-dimensional CAs. Hereafter, we discuss the patterns generated by Sym-2dECAs with $(a,b)=(0,1)$.

4.1 346 spatio-temporal patterns generated by 1024 Sym-2dECAs

The 1024 Sym-2dECAs with $(a,b)=(0,1)$ generate fractal-like spatio-temporal patterns from the single site seed configuration x_o. However, do not generate a set of 1024 different patterns, because in some cases some transitions of local rules are not used. This means that we can choose two different Sym-2dECAs $(A^{\mathbb{Z}^2},F)$ and $(A^{\mathbb{Z}^2},\tilde{F})$ such that $\{F^n x_o\}_{n\geq0}=\{\tilde{F}^n x_o\}_{n\geq0}$.

Here, we study the existence of the different types of spatio-temporal patterns in 1024 Sym-2dECAs. Figure 8 presents the numerical results of this study. The horizontal axis represents the time steps n from 0 to 1024, and the vertical axis represents the number of different spatio-temporal patterns generated. This is a semilog graph, defined by a logarithmic scale on the horizontal axis and a linear scale on the vertical axis. When the time step $n=0$, the number of different spatio-temporal patterns is just one, because all spatio-temporal patterns start with the single site seed x_o. The number gradually increases, because we can distinguish some spatio-temporal patterns step by step. When $n=86$, the number reaches 346. Following this, it does not increase until $n=1024$. Thus, we obtain the following result:

Result 4.1. *For the* 1024 *spatio-temporal patterns generated by Sym-2dECAs with* $(a,b)=(0,1)$*, it is numerically shown that there exist* 346 *different spatio-temporal patterns* $\{F^n x_o\}^{1024}_{n=0}$.

In Result 4.1, the study is restricted until the time step 1024 because of the computational limitations of the computer that was utilized. Therefore, we know that there are at least 346 different patterns $\{F^n x_o\}_{n\in\mathbb{N}}$. Among the 346 spatio-temporal patterns, 300 patterns are generated by a single Sym-2dECA, and each of the other 46 are generated by multiple CAs. Table 2 lists the latter 46 CA rules. In Table 2, the notation "$*$" represents either 0 or 1, which means that some transitions are ignored for creating the patterns. We name each local rule from $\langle 5a\rangle$ through to $\langle 11n\rangle$, where the number represents the number of transitions used when creating the patterns and the letter represents the rules in alphabetical order.

4.2 Relation between the 346 spatio-temporal patterns and the singular function

Now, we study the 346 spatio-temporal patterns. It is difficult to calculate the fractal dimension of each pattern directly, although they have a fractal-like appearance. Instead of this, we adopt the

Table 2: The 46 rules of Sym-2dECAs based on the spatio-temporal patterns from a single site seed. Here, we show the rules depending on fewer than 12 transitions. The asterisk symbol ($*$) represents either 0 or 1. We name each local rule from $\langle 5a \rangle$ through to $\langle 11n \rangle$, where the number represents the number of transitions used when creating the patterns and the letter represents the rules in alphabetical order.

T	0	0	0	1	0	1	0	0	0	1	0	1
LCR	000	000	001	000	101	101	010	010	011	010	111	111
B	0	1	1	1	1	1	0	1	1	1	1	1
$\langle 5a \rangle$	$*$	$*$	$*$	$*$	$*$	1	0	$*$	0	$*$	0	1
$\langle 5b \rangle$	$*$	$*$	$*$	$*$	$*$	1	1	$*$	1	$*$	0	1
$\langle 6a \rangle$	$*$	$*$	$*$	$*$	$*$	1	0	$*$	1	0	0	1
$\langle 6b \rangle$	$*$	$*$	$*$	$*$	$*$	1	1	0	0	$*$	0	1
$\langle 7a \rangle$	0	$*$	0	$*$	0	0	$*$	$*$	0	$*$	0	1
$\langle 7b \rangle$	$*$	$*$	$*$	$*$	$*$	1	0	0	1	1	0	1
$\langle 7c \rangle$	$*$	$*$	$*$	$*$	$*$	1	0	1	1	1	0	1
$\langle 7d \rangle$	$*$	$*$	$*$	$*$	$*$	1	1	1	0	0	0	1
$\langle 7e \rangle$	$*$	$*$	$*$	$*$	$*$	1	1	1	0	1	0	1
$\langle 7f \rangle$	1	$*$	$*$	$*$	1	0	1	$*$	1	$*$	0	1
$\langle 8a \rangle$	1	$*$	$*$	$*$	0	0	1	1	1	$*$	0	1
$\langle 9a \rangle$	0	$*$	$*$	0	0	0	1	1	1	$*$	0	1
$\langle 9b \rangle$	0	$*$	1	0	0	0	0	$*$	1	$*$	0	1
$\langle 9c \rangle$	0	1	$*$	$*$	1	0	1	$*$	1	1	0	1
$\langle 9d \rangle$	0	1	1	$*$	1	0	0	$*$	0	$*$	0	1
$\langle 9e \rangle$	1	0	0	$*$	0	0	1	$*$	0	$*$	0	1
$\langle 10a \rangle$	0	0	0	0	1	0	0	$*$	0	$*$	0	1
$\langle 10b \rangle$	0	0	0	1	1	0	0	$*$	0	$*$	0	1
$\langle 10c \rangle$	0	$*$	$*$	1	1	0	1	1	1	0	0	1
$\langle 10d \rangle$	0	0	1	0	0	0	0	$*$	0	$*$	0	1
$\langle 10e \rangle$	0	0	1	0	1	0	0	$*$	0	$*$	0	1
$\langle 10f \rangle$	0	0	1	1	0	0	0	$*$	0	$*$	0	1
$\langle 10g \rangle$	0	0	1	1	1	0	0	$*$	0	$*$	0	1
$\langle 10h \rangle$	0	1	0	0	1	0	0	$*$	0	$*$	0	1
$\langle 10i \rangle$	0	1	0	1	1	0	0	$*$	0	$*$	0	1
$\langle 10j \rangle$	0	1	1	0	0	0	0	$*$	0	$*$	0	1
$\langle 10k \rangle$	0	1	1	$*$	1	0	1	0	0	$*$	0	1
$\langle 10l \rangle$	0	1	1	1	0	0	0	$*$	0	$*$	0	1
$\langle 10m \rangle$	1	0	0	$*$	0	0	0	0	0	$*$	0	1
$\langle 10n \rangle$	1	0	$*$	0	0	0	0	1	1	$*$	0	1
$\langle 10o \rangle$	1	1	1	$*$	1	0	0	0	0	$*$	0	1
$\langle 10p \rangle$	1	1	1	$*$	1	0	1	0	0	$*$	0	1
$\langle 11a \rangle$	0	0	0	0	0	0	0	0	1	$*$	0	1
$\langle 11b \rangle$	0	0	0	0	0	0	0	1	1	$*$	0	1
$\langle 11c \rangle$	0	0	0	0	0	0	1	0	1	$*$	0	1
$\langle 11d \rangle$	0	0	$*$	0	1	0	1	1	1	1	0	1
$\langle 11e \rangle$	0	0	$*$	1	0	0	1	1	1	1	0	1
$\langle 11f \rangle$	0	0	$*$	1	1	0	1	1	1	1	0	1
$\langle 11g \rangle$	0	1	$*$	1	0	0	1	1	1	0	0	1
$\langle 11h \rangle$	0	1	$*$	1	0	0	1	1	1	1	0	1
$\langle 11i \rangle$	1	0	0	0	0	0	1	0	1	$*$	0	1
$\langle 11j \rangle$	1	1	0	0	0	0	1	0	0	$*$	0	1
$\langle 11k \rangle$	1	1	0	$*$	0	0	1	1	0	1	0	1
$\langle 11l \rangle$	1	1	0	1	0	0	1	0	0	$*$	0	1
$\langle 11m \rangle$	1	1	1	$*$	1	0	1	1	0	0	0	1
$\langle 11n \rangle$	1	1	1	$*$	1	0	1	1	0	1	0	1

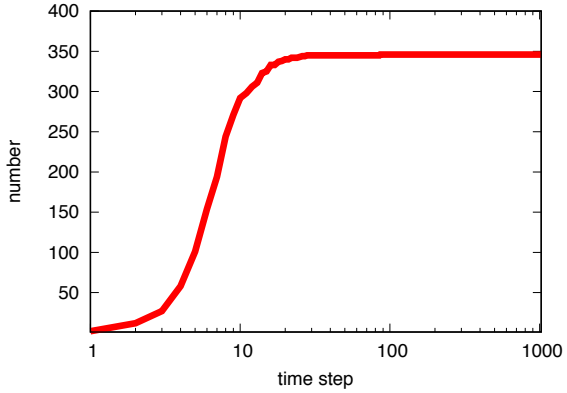

Figure 8: The number of different spatio-temporal patterns for 1024 Sym-2dECAs with $(a, b) = (0, 1)$. The horizontal axis shows the time step n from 0 to 1024, and the vertical axis shows the number of different spatio-temporal patterns. This is a lin-log plot.

analysis method for Sym-2dECA (5) presented in [3, 8]. We count the number of cells that form the pattern for each time step. Let

$$num(n) = \sum_{(i,j)\in\mathbb{Z}^2} 1 - (F^n x_o)_{i,j}, \quad cum(n) = \sum_{k=0}^{n} num(k). \tag{19}$$

The notation $num(n)$ for the time step $n \in \mathbb{N}$ represents the number of "0" states in $F^n x_o$, and $cum(n)$ represents the cumulative sum of the number of "0" states in $F^n x_o$ from the time step 0 to n. We can plot the graphs of $\{num(n)\}_{n\in\mathbb{N}}$ and $\{cum(n)\}_{n\in\mathbb{N}}$ for the 346 patterns and observe the evolution.

Most of the graphs of $\{num(n)\}_{n\in\mathbb{N}}$ are gradually monotonically increasing, but some appear to be self-similar or self-affine. In particular, for some Sym-2dECAs we can observe that the CAs are related to the singular function (6). There exist six patterns for which $\{num(n)\}_{n\in\mathbb{N}}$ is well represented by the singular function $L_{1/4}$. For the graphs of $\{cum(n)\}_{n\in\mathbb{N}}$, there exist two patterns for which the cumulative number of the "0" states is represented by the singular function $L_{1/5}$. The graphs in Figure 9 show the evolution of the number of cells that comprise the pattern $\langle 5b\rangle$. Figure 9 (a) presents the graph of $num(n)$ from the time step 0 to 256. The curve is jagged overall, and following initial small fluctuations the number fluctuates drastically. On the other hand, Figure 9 (b) shows the graph of $cum(n)$ from the time step 0 to 256. The curve is smooth almost everywhere, and it can be exactly replicated by the singular function (6) with the parameter $\alpha = 1/5$.

We obtain the following result:

Result 4.2. *Among the* 346 *different spatio-temporal patterns of Sym-2dECAs with* $(a, b) = (0, 1)$*, the following observations hold:*

1. $\{num(n)\}_{n\in\mathbb{N}}$ *of the Sym-2dECAs for* $\langle 9a\rangle$, $\langle 10c\rangle$, $\langle 10n\rangle$, $\langle 11d\rangle$, $\langle 11e\rangle$, *and* $\langle 11g\rangle$ *in Table 2 are described by the singular function* L_α *with the parameter* $\alpha = 1/4$.

2. $\{cum(n)\}_{n\in\mathbb{N}}$ *of the Sym-2dECAs for* $\langle 5b\rangle$ *and* $\langle 7f\rangle$ *in Table 2 are described by the singular function* L_α *with* $\alpha = 1/5$.

The rule of the Sym-2dECA (5) is included for the case of $\langle 10c\rangle$ in Table 2. Result 4.2.*1* represents a generalization of the result given for the CA in [3, 8]. The spatio-temporal patterns of the Sym-2dECAs in Result 4.2 are illustrated in Figures 10 and 11. Figure 10 $\langle 10c\rangle$ show the patterns of the Sym-2dECA (5). We can observe that the other patterns in Figure 10 are similar to those in $\langle 10c\rangle$. In particular, for odd time steps the spatio-temporal patterns of $\langle 9a\rangle$ and $\langle 10n\rangle$ are exactly the same as those of $\langle 10c\rangle$. For even time steps, the spatio-temporal patterns of $\langle 11d\rangle$ are the same as those

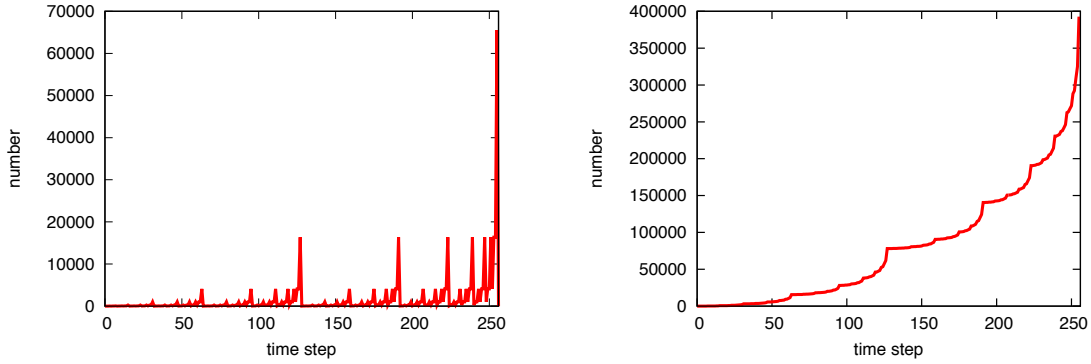

(a) Graph of $\{num(n)\}_{n=0}^{256}$ (b) Graph of $\{cum(n)\}_{n=0}^{256}$

Figure 9: Graphs of $\{num(n)\}_{n=0}^{256}$ and $\{cum(n)\}_{n=0}^{256}$ for the pattern $\langle 5b \rangle$ in Table 2.

of $\langle 10c \rangle$. The patterns of $\langle 11e \rangle$ and $\langle 11g \rangle$ are different, but for odd time steps the boundaries of the patterns are very similar. The features of the patterns in Figure 11 are different from those in Figure 10. In the patterns of both $\langle 5b \rangle$ and $\langle 7f \rangle$, one can observe combinations of simple square-shaped clusters. These expand in a row, and are sometimes separated during growth.

In addition to Result 4.2.*2*, we obtain recurrence formulas for $\{num(n)\}_{n\in\mathbb{N}}$ for the two spatio-temporal patterns $\langle 5b \rangle$ and $\langle 7f \rangle$. We do not yet possess rigorous mathematical proofs for the relations between the numbers and the singular functions, but we can represent the numbers using the following recurrence formulas:

Remark 4.1. *The recurrence formulas for $\{num(n)\}_{n\in\mathbb{N}}$ for $\langle 5b \rangle$ and $\langle 7f \rangle$ are obtained as follows:*

1. *For the Sym-2dECA in $\langle 5b \rangle$, the number $p_n := num(n)$ is obtained from $p_n = 4^{q_n}$, where*

$$q_0 = 0, \quad q_{2^k+m} = \begin{cases} 1 & \text{if } m = 0, \\ q_{2^k+m-1} + q_m - q_{m-1} & \text{otherwise,} \end{cases}$$

   for $k \geq 0$, where $0 \leq m < 2^k$. We can easily find that if $m = 2^l$ $(0 \leq l < k)$, then $q_{2^k+m} = 2$.

2. *For the Sym-2dECA in $\langle 7f \rangle$, the number $r_n := num(n)$ is obtained from $r_0 = 1$, $r_1 = 5$, and $r_{2^k+m} = 4r_m$ $(k \geq 1,\ 0 \leq m < 2^k)$.*

In our previous study, we presented the relation between the one-dimensional elementary cellular automaton Rule 90 and the singular function with $\alpha = 1/3$ [16]. For the spatio-temporal pattern of the CA from a single site seed, the number of "0" states was described as a function $L_{1/3}$. This result implies that the relation between the CA and the singular function is not uncommon in CA studies. Thus, we can expect that several other CA patterns are generally governed by the singular function, because we observe these results regardless of the dimension, linearity, and so on.

From these observations, we are led to Conjecture 4.1.

Conjecture 4.1. *For a Sym-2dECA $(A^{\mathbb{Z}^2}, F)$, we propose that the following hold:*

1. *If the limit $\lim_{m\to\infty} \{num(n)/num(2^m)\}_{0\leq n\leq 2^m}$ exists and is represented by the singular function L_α for some α $(0 < \alpha < 1,\ \alpha \neq 1/2)$, then the box-counting dimension of the limit set of the spatial pattern is as follows:*

$$dim_B \left(\lim_{m\to\infty} F^{2^m} x_o \right) = -\frac{\log \alpha}{log2}; \tag{20}$$

2. *If the limit $\lim_{m\to\infty} \{cum(n)/cum(2^m)\}_{0\leq n\leq 2^m}$ exists and is represented by the singular function L_α for some α $(0 < \alpha < 1,\ \alpha \neq 1/2)$, then the box-counting dimension of the limit set of*

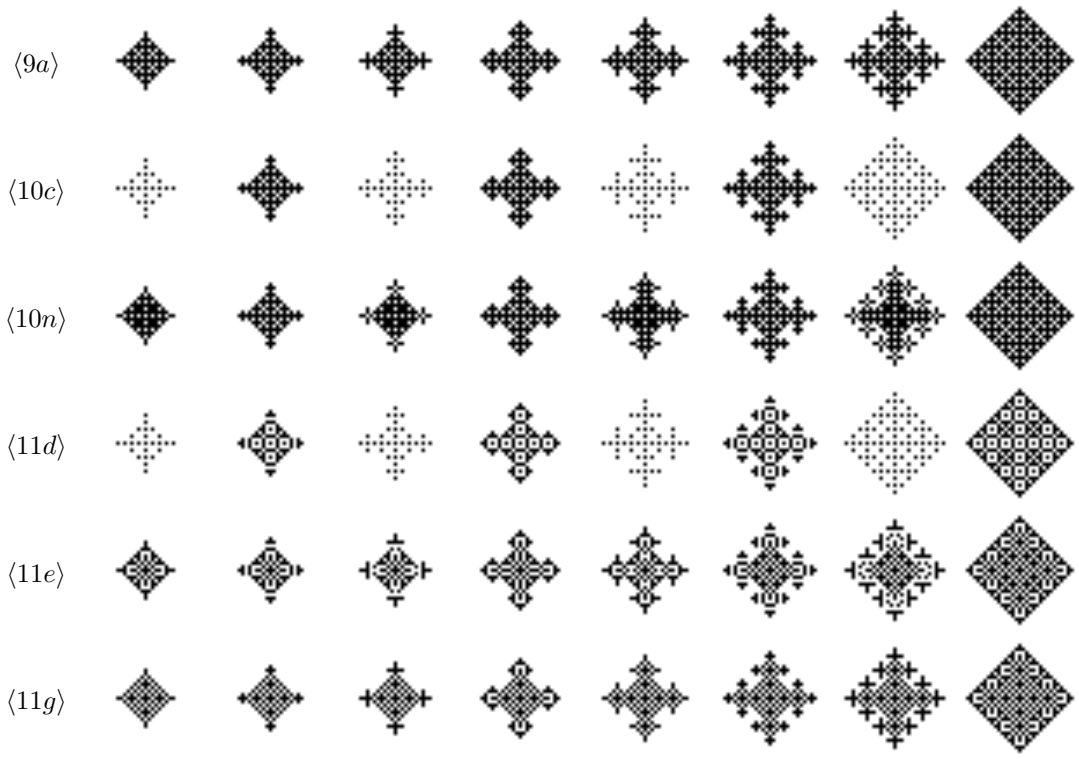

Figure 10: Time evolution of $\{F^n x_o\}_{n=8}^{15}$ in Result 4.2.*1*.

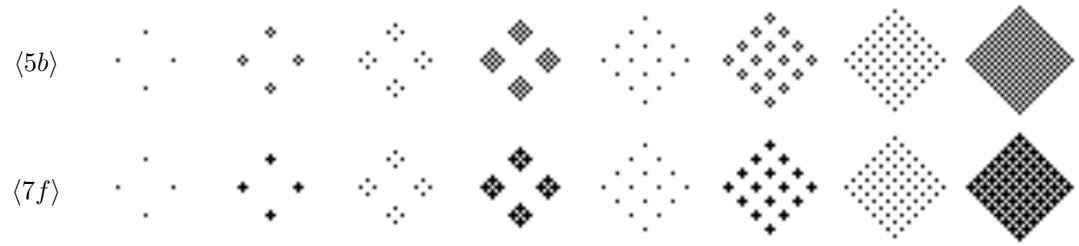

Figure 11: Time evolution of $\{F^n x_o\}_{n=8}^{15}$ in Result 4.2.*2*.

the spatio-temporal pattern is as follows:

$$dim_B \left(\lim_{m\to\infty} \bigcup_{k=0}^{2^m} F^k x_o \right) = -\frac{\log \alpha}{log 2}. \tag{21}$$

5 Conclusion

We have investigated the fractal structures generated by symmetrical two-dimensional cellular automata. In our previous studies [3, 8], we had determined numerically that the spatio-temporal pattern has a fractal-like structure, and the proof of this result was presented in [4].

In this paper, we first provided an overview of the existence of a limit set for a cellular automaton and described the fractal dimension (box-counting dimension) of the boundary of the spatial pattern. We employed the relation between the patterns and a singular function to obtain the result. We represented the patterns by unions of squares K_n, and we calculated their surfaces. Next, we provided numerical results concerning the fractal structures of symmetrical two-dimensional elemen-

tary cellular automata. Within that class, there were 1024 cellular automata that created fractal-like patterns, and there were 346 different types of spatio-temporal patterns from the single site seed. In addition, we found that for six of the patterns the number of cells comprising them was described by the singular function with the parameter 1/4 (this result generated a previous result for a particular automaton). Furthermore, for two of the patterns, the cumulative sum of the number of the cells was described by the function with the parameter 1/5. In our previous study, we proved that the fractal structure for a one-dimensional elementary cellular automaton Rule 90 could be described by the singular function with the parameter 1/3 [16]. The parameter α depends on the self-similarity of the limit set generated by a cellular automaton rule. In the case of Rule 90, the limit set comprises three half-sized subsets of the full limit set. This similarity determines the parameter 1/3. However, in the case of the two-dimensional ECA90 in Result 4.2.*2*, the limit set comprises five half-sized subsets of the full limit set, and this means that $\alpha = 1/5$. We can regard these results as an application to other spatio-temporal patterns. We expect that some of the patterns with fractal structures can be characterized or classified by the singular function with the parameter α. Based on all of our results, we expect that there will be more hidden general relations between cellular automata and singular functions. In fact, in symmetrical two-dimensional elementary cellular automata, we numerically observed many spatio-temporal patterns that were "nearly" characterized by the singular function. This indicates that this particular class of cellular automata is basically related to the singular function. In the future, we will study the details of this relation. Further applications and proofs will be reported elsewhere.

References

[1] S. J. Willson. Cellular automata can generate fractals. *Discrete Applied Mathematics*, 8(1):91 – 99, 1984.

[2] S. Takahashi. Cellular automata and multifractals: dimension spectra of linear cellular automata. *Phys. D*, 45(1 – 3):36 – 48, 1990.

[3] A. Kawaharada. Ulam's cellular automaton and rule 150. *Hokkaido Mathematical Journal*, 43:361 – 383, 2014.

[4] A. Kawaharada and T. Namiki. Fractal structure of a class of two-dimensional two-state cellular automata. *Proceedings of International Workshop on Applications and Fundamentals of Cellular Automata 2017*, pages 205 – 208, 2017.

[5] M. Yamaguti, M. Hata, J. Kigami, and translated by Kiki Hudson. *Mathematics of fractals*. American Mathematical Society, 1997.

[6] M. Hata and M. Yamaguti. The Takagi function and its generalization. *Japan J. Appl. Math.*, 1(1):183 – 199, 1984.

[7] R. Salem. On some singular monotonic functions which are strictly increasing. *Trans. Amer. Math. Soc.*, 53:427 – 439, 1943.

[8] A. Kawaharada. Fractal patterns created by Ulam's cellular automaton. *Proceedings of International Workshop on Applications and Fundamentals of Cellular Automata 2014*, pages 484 – 486, 2014.

[9] S. Ulam. On some mathematical problems connected with patterns of growth of figures. *the Proceedings of Symposia in Applied Mathematics*, 14:215–224, 1962.

[10] G. d. Rham. Sur quelques courbes definies par des equations fonctionnelles. *Univ. e Politec. Torino. Rend. Sem. Mat.*, 16:101–113, 1956/1957.

[11] K. Kawamura. On the set of points where Lebesgue's singular function has the derivative zero. *Proc. Japan Acad. Ser. A Math. Sci.*, 87(9):162–166, 2011.

[12] Z. Lomnicki and S. Ulam. Sur la théorie de la mesure dans les espaces combinatoires et son application au calcul des probabilités i. variables indépendantes. *Fund. Math.*, 23:237 – 278, 1934.

[13] B. B. Mandelbrot. *The Fractal Geometry of Nature*. W. H. Freeman and Co., 1982.

[14] K. Falconer. *Fractal Geometry: Mathematical Foundations and Applications*. Wiley, 2003.

[15] S. Takahashi. Self-similarity of linear cellular automata. *Journal of Computer and System Sciences*, 44:114 – 140, 1992.

[16] A. Kawaharada and T. Namiki. Cumulative distribution of rule 90 and lebesgue's singular function. *Proceedings of AUTOMATA 2014*, pages 165 – 169, 2014.

Acknowledgment

This work is partly supported by the Grant in Aid for Scientific Research 15K17591, 16K13772, and 15H05878.